MRS Communications (2013), *3*, 245–248
© Materials Research Society, 2013
doi:10.1557/mrc.2013.39

MRS Communications

Research Letters

Reversible dislocation motion and microcracking in plastically anisotropic solids under cyclic spherical nanoindentation

B. Anasori and **M.W. Barsoum,** Department of Materials Science and Engineering, Drexel University, Philadelphia, Pennsylvania 19104
Address all correspondence to B. Anasori at **anasori@drexel.edu**

(Received 7 May 2013; accepted 11 September 2013)

Abstract

Recently, fully reversible dislocation motion was postulated to result in hysteretic nanoindentation load–displacement loops in plastically anisotropic solids. Since microcracking can also result in hysteretic loops, here we define a new parameter, reversible displacement (*RD*) that can differentiate between the two. For C-plane $LiTaO_3$ surfaces and five other plastically anisotropic solids, the *RD* values either increase initially or remain constant with cycling. In contradistinction, for glass and A-plane ZnO surfaces, where energy dissipation is presumably due to microcracking or irreversible dislocation pileups, respectively, the *RD* values decreased continually with cycling.

Over the past half dozen years we have shown that many plastically anisotropic materials, in which dislocations are confined to two-dimensions, outline fully and spontaneously reversible hysteretic stress–strain loops upon cyclic loading. We postulated that the micromechanism for this phenomenon is the formation and annihilation of multiple, co-axial parallel dislocation loops, whose shape guarantees that they only remain open when a load is applied; unloading results in their shrinkage and/or their annihilation.[1–4] Among others, we have shown that a large number of seemingly unrelated solids such as C-plane ZnO,[5] $BaTiO_3$,[6] sapphire,[7] $LiNbO_3$,[8] $LiTaO_3$,[9] Mg, Co, Ti, Zn,[10,11] graphite,[12] mica,[2,13] and the MAX phases,[3] trace fully reversible hysteretic stress–strain loops upon cyclic loading.

Working mostly with single crystals, we showed that when one of the aforementioned materials is indented with a spherical indenter, a linear elastic regime is usually followed, in most cases, by pop-in events, that in some cases are massive, followed, after a few cycles, by fully and spontaneously reversible hysteretic load–displacement curves.[13] During the pop-in events, the strain energy released results in the creation of a multitude of nanodomains and, in the case of $LiNbO_3$ and $LiTaO_3$, twins.[8,9] When the nanoindenter is reloaded into the *same* location, we postulated that coaxial dislocation loops nucleate within the domains formed during the pop-ins. The reversible motion, of these dislocations in turn, is believed to result in the energy dissipated per unit volume per cycle, W_d. The presence of microdomains—that play the role of grain boundaries in polycrystalline solids—that do not allow the parallel dislocation loops to dissociate into mobile dislocation walls (MDWs) is thus essential for their reversible behavior.[5,7–9]

Previously, we referred to these co-axial, parallel dislocation loops as incipient kink bands (IKBs). Materials that dissipated energy via this mechanism were labeled kinking nonlinear elastic (KNE) solids.[1–4] In sharp contradistinction to other energy-dissipating mechanisms in crystalline solids, such as microcracking or phase transitions, KNE solids have excellent fatigue resistance. For example, it is possible to indent sapphire single crystals in the same location to stresses of the order of 40 GPa, 24 times and observe *no* measurable differences in the shape and/or area of the reversible load–displacement loops after the ≈6th cycle.[7]

The W_d values measured for $LiTaO_3$ were some of the highest of any single crystals examined so far.[2,5,7–9,12,13] The reason for this state of affairs is believed to be the formation of twins [see supplementary Fig. S1(a)]—during the early stages of deformation and/or the pop-in events—that rotate domains into an orientation that is more amenable to reversible dislocation motion (RDM) within the basal planes.[8,9]

There are also some reports on microcracking as the origin of hysteretic load–displacement loops. Richter et al.[14] ascribed the hysteretic load–displacement loops in MgO single crystals to microcracking. The latter can cause some energy dissipation but typically fades with cycling. Oliver and Pharr[15] reported hysteretic load–displacement loops during the early stages of nanoindentation (NI) in soda lime glass, which also degenerated with cycling.

This work's main goal is to differentiate between RDM and other energy-dissipating mechanisms, such as microcracking or irreversible dislocation pileups. To do so, two diamond hemispherical indenters with radii, *R*, of 5 and 21 μm, were loaded into the same location—on a C-plane $LiTaO_3$, a plastically anisotropic solid, and a soda-lime glass microscope slide, an

https://doi.org/10.1557/mrc.2013.39 Published online by Cambridge University Press

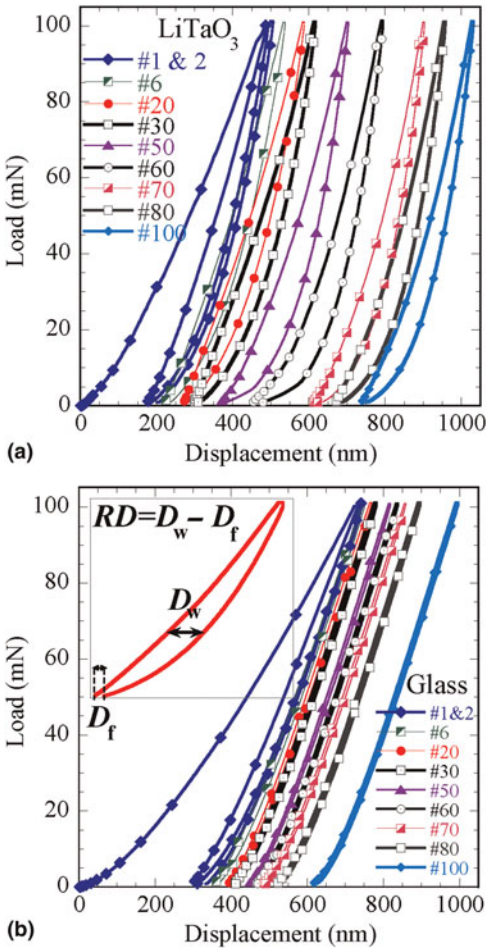


Figure 1. (a) Select NI load–displacement curves for a given location loaded 100 times to 100 mN with the 5 μm radius indenter on, (a) a C-plane $LiTaO_3$ single crystal, (b) a glass slide. The top inset in (b) shows a schematic of how *RD* is calculated from each load–displacement loop.

amorphous material—100 times to stresses, of the order of 6–9 GPa, while concomitantly recording the load–displacement curves. The loading rate/load ratio was kept constant at 0.1. To maintain contact between the indenter and the specimen, each of the unloading cycles were interrupted at 1% of the maximum load. During some NI runs, and despite waiting for the nanoindenter to settle down, instrumental drift, both positive and negative, were observed. The origin of the instrumental drift can be the result of temperature changes during the test. This was noted despite the fact that the tests were started only when the drift was below 0.05 nm/s. Thus, the maximum drift on each cycle was about ±5 and ±7.5 nm for 5 and 21 μm indenters, respectively. Needless to add, this drift can influence the load–displacement and complicate the analysis. The technique we are proposing here also minimizes the influence of drift.

Typical NI load–displacement cycles obtained when the 5 μm radius tip was indented 100 times into the same location in $LiTaO_3$ and the glass slide are shown in Figs. 1(a) and 1(b), respectively. For the sake of clarity, only select cycles are plotted. In Fig. 1(a), as in all our previous work on KNE solids, the first loop is open; subsequent loops, up to cycle 6, are open, but successively less so. From the 6th to ≈35th cycles, the loops are closed and fully reversible. Cycling beyond 35 times, results in larger, open loops until around cycle 75, after which the loops close and become reversible again. The load–displacement plots are different on the glass sample; the first loop is open and the subsequent loops are small and become smaller up to cycle 10. From the 10th cycle through the end of the test (cycle 100th) the loops are quite small and their areas remain more or less constant.

The first cycle load–displacement curves in both samples are quite comparable. In most of our previous NI work, to further analyze the results and differentiate between reversible dislocation motion and other reasons for energy dissipation, we converted the NI results to NI cyclic stress–strain curves. This conversion entailed some assumptions and approximations that some have questioned. Here, to avoid this problem, we define a new parameter, viz. reversible displacement (*RD*)—shown schematically in the inset in Fig. 1(b)—as:

$$RD = D_w - D_f$$

where D_w is the maximum width of each loop and D_f is the non-reversible displacement at the end of each cycle. It follows that *RD* is a measure of the *reversible* energy dissipation during each cycle regardless of its origin. As shown below, plotting *RD* versus cycle number is a powerful, simple and straightforward method to differentiate between these two damping phenomena.

Figure 2(a) plots *RD* versus cycle number for both the $LiTaO_3$ and the glass samples loaded 100 times to 100 and 550 mN with the 5 and 21 μm indenters, respectively. The results on two different locations are shown for each sample and tip size. At about 13 ± 1 nm, the *RD* on the glass slide, for the 5 μm tip, has its maximum value during cycle 2, and decreases to ≈3 ± 3 nm after ≈10 cycles and remains constant throughout the rest of the test. For the 21 μm tip, the *RD* starts around 17 ± 1 nm, and decreases to the same minimum value (≈3 ± 3 nm) as for the 5 μm tip, also after ≈10 cycles. In general, for both indenter sizes and for all the locations the *RD*s on the glass showed two stages: a decrease from a maximum value at the very beginning to a steady-state regime after ≈10 cycles after which it remained constant at ≈3 ± 3 nm. Note that the steady-state regime is achieved more or less after the same cycle numbers for both indenter sizes.

In sharp contradistinction to the glass surface, the *RD* response versus cycle number for $LiTaO_3$—for both indenter sizes in two different locations represented by blue and purple curves, respectively, in Fig. 2(a)—is qualitatively and quantitatively different. Here, the *RD*s start at a low value, go through a maximum around cycle 40 for the 5 μm indenter tip (blue and purple curves in center of Fig. 2(a)) and ten cycles for the 21 μm indenter tip [top blue and purple curves in Fig. 2(a)] before

https://doi.org/10.1557/mrc.2013.39 Published online by Cambridge University Press

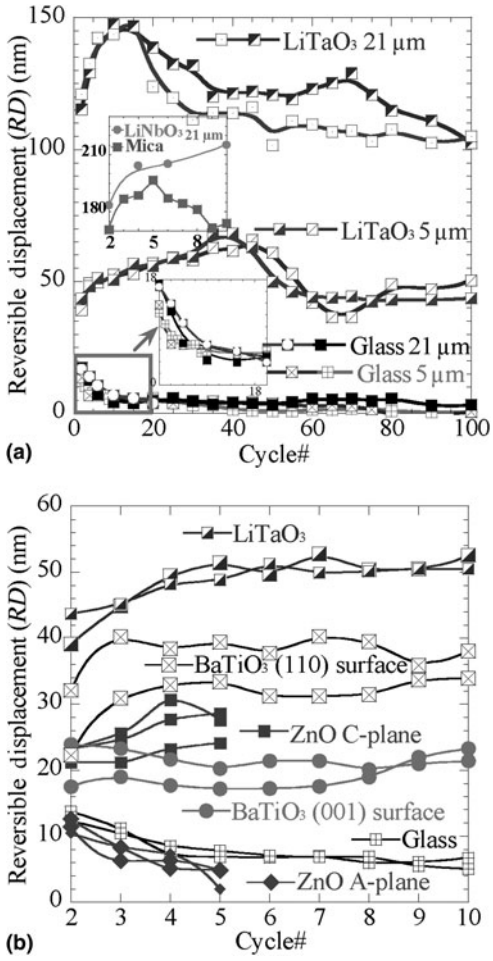


Figure 2. *RD* versus cycle number for (a) two different locations on the $LiTaO_3$ and glass surfaces loaded 100 times to 100 mN with the 5 μm indenter and 550 mN with the 21 μm indenter. The top inset shows the RD values for $LiNbO_3$ and mica loaded 10 times to 550 mN with 21 μm tip, (b) up to cycle 10th for two locations on $LiTaO_3$ and the glass sample indented to 100 mN with the 5 μm indenter. Also plotted are the *RD* values for A- and C-plane ZnO single crystals,[5] (001) and (110) $BaTiO_3$ surfaces,[6] and indented with a 13.5 μm indenter.

gradually decreasing to the 100th cycle. When the *RD*s for $LiNbO_3$ are plotted for cycles 2–10, a similar trend is observed [top inset in Fig. 2(a)].

The two diametrically opposite responses of *RD* with cycling [Fig. 2(a)], for the glass and $LiTaO_3$, are fully consistent with our understanding of the nature of the energy dissipated in each material. In the glass, microcracking and the concomitant friction between the crack surfaces is the only possible energy-dissipating mechanism. Since cycling would tend to wear and smoothen cracked surfaces, it is not surprising that friction between these surfaces decreases with cycling which in turn leads to a reduction in the *RD* and W_d values. Note that another factor could be the reduction in stress under the indenter as the microcracks increase in size with cycling. Scanning electron microscopy (SEM) micrographs of the indentation in the glass after 2, 10, and 100 cycles (see Fig. S3, in supplementary material) suggest that if the area changes with cycling, such changes are quite small. This comment notwithstanding, in either case, *RD decreases* with cycling. It is thus quite significant that the *RD*s for $LiTaO_3$ initially *increase* with cycling. The latter implies that although microcracks exist around the indentation mark in $LiTaO_3$ even after a few cycles [see Fig. S1(a) in supplementary material] the mechanism responsible for the *RD* in $LiTaO_3$ cannot be solely due to microcracking; another mechanism, that is much more dissipative, must be invoked.

Over the years, we have made the case that a possible second mechanism is in the form of IKBs. The results shown in Fig. 2(a) support this notion. We have shown in our previous NI work that in both $LiTaO_3$[9] and $LiNbO_3$[8] during the pop-in stage $(10\bar{1}2)[10\bar{1}1]$ twins form [see Figs. S1(a) and S1(b) in supplementary material]. The latter rotate the basal planes in orientations that are more amenable to dislocation movement (see supplementary Fig. S2) that in turn result in the largest reversible NI loops we have ever measured.[8,9] The initial increase in *RD* with cycling can thus be ascribed to this reorienation and its cyclic dependence.

Note that the conclusion that RDM results in hysteretic loops does not neccesarily rule out microcracking. It is reasonable to assume that the reduction in *RD* past its peak values for both indenters [Fig. 2(a)] is related to the nucleation and growth of microcracks. Indeed, post-SEM micrographs of indented regions more often than not show a plethora of microcracks, especially after 100 cycles [see Fig. S1(d) in supplementary material].

To test the general validity of this conclusion we revisited our results on the cyclic loading of $LiTaO_3$,[9] $LiNbO_3$,[8] (110) and (001) $BaTiO_3$,[6] mica,[13] and A- and C-plane ZnO surfaces.[5] Figure 2(b) plots the *RD* versus cycle number for these diverse solids. The *RD* values for mica and $LiNbO_3$ are plotted in Fig. 2(a). Also plotted, for comparison, are the results obtained on glass obtained here. A perusal of these results quickly establishes that with the exception of the glass and ZnO A-plane—in which the *RD*s decrease with cycle number—for all of the other surfaces, the *RD*s either increase, or remain constant as in the case of the (001) $BaTiO_3$ surface with cycle number. Gratifyingly, the latter surfaces were all classified as KNE based on our analysis of their NI stress–strain curves.

The results on the ZnO A-plane are noteworthy. Based on our NI results[5] and, more importantly, those of others[16] we concluded that in this orientation, *irreversible dislocation pile-ups* and *not* IKBs nucleated under the indenter. The latter were seen in cross-sectional transmission electron microscopy (TEM) micrographs.[5,16] Clearly, the *RD* result for this ZnO orientation is more reminiscent of the glass surface. However, in this case, the energy dissipation cannot be ascribed to microcracks for the simple reason that none were observed in post-indentation SEM observations of the indentation marks.[5] This is an important result because it suggests that pileup reversibility also fades with cycling, presumably as a result of work

https://doi.org/10.1557/mrc.2013.39 Published online by Cambridge University Press

hardening. It is worth re-emphasizing here that cracks were *not* observed when the C-plane ZnO surfaces were cyclically indented (see Fig. S4 in supplementary materials) which rules out microcracking in that case.

The advantages of measuring *RD* are that only the raw load–displacement data are used. There are also some reports on measuring the full-width at half-maximum (FWHM) of the load–displacement loops during cyclic indentation.[6,17] We believe that *RD* is more accurate and powerful than FWHM because, (a) the D_w does not always occur at half maximum, and (b) during high cycle indentation tests, the drift can be problematic. By subtracting the D_f from D_w the effect of the drift is minimized (see supplementary material).

In conclusion, here, we define a new parameter, *RD*, which is related to, and indirectly measures, the reversible deformation of a region below a spherical nanoindenter. By plotting the *RD* versus the number of cycles two different responses were observed. The first was a gradual decrease in *RD* with cycling; the second was an initial gradual increase or a constancy with cycle number. The former was correlated with microcracking or irreversible dislocation pileups; the latter with RDM, most likely in the form of IKBs. By using this technique, we re-confirmed that $LiTaO_3$, $LiNbO_3$, $BaTiO_3$, C-plane ZnO, and mica single crystals are KNE solids. More importantly, we also show that the energy dissipation in glass and A-plane ZnO decrease or fade with cycling, and are thus not due to RDM. Finally, it is important to note that the conclusions reached here are *not* contingent on the existence of IKBs; the conclusions reached, apply to any form of RDM.

Supplementary materials

For supplementary material for this article, please visit http://dx.doi.org/10.1557/mrc.2013.39

Acknowledgment

This work was supported by the Army Research Office (grant no. W911NF-11-01-0525).

References

1. F.C. Frank and A.N. Stroh: On the theory of kinking. *Proc. Phys. Soc.* **65**, 811–821 (1952).
2. M.W. Barsoum, A. Murugaiah, S.R. Kalidindi, and T. Zhen: Kinking nonlinear elastic solids, nanoindentations, and geology. *Phys. Rev. Lett.* **92**, 255508 (2004).
3. A.G. Zhou, M.W. Barsoum, S. Basu, S.R. Kalidindi, and T. El-Raghy: Incipient and regular kink bands in fully dense and 10 vol.% porous Ti_2AlC. *Acta Mater.* **54**, 1631–1639 (2006).
4. M.W. Barsoum, T. Zhen, S.R. Kalidindi, M. Radovic, and A. Murugaiah: Fully reversible, dislocation-based compressive deformation of Ti_3SiC_2 to 1 GPa. *Nat. Mater.* **2**, 107–111 (2003).
5. S. Basu, M.W. Barsoum: Deformation micromechanisms of ZnO single crystals as determined from spherical nanoindentation stress–strain curves. *J. Mater. Res.* **22**, 2470–2477 (2007).
6. R. Buchs, S. Basu, O.A. Elshrief, R. Coward, and M.W. Barsoum: Spherical nanoindentation and Vickers microhardness study of the deformation of poled $BaTiO_3$ single crystals. *J. Appl. Phys.* **105**, 093540 (2009).
7. S. Basu, M.W. Barsoum, and S.R. Kalidindi: Sapphire: a kinking nonlinear elastic solid. *J. Appl. Phys.* **99**, 063501 (2006).
8. S. Basu, A.G. Zhou, and M.W. Barsoum: Reversible dislocation motion under contact loading in $LiNbO_3$ single crystal. *J. Mater. Res.* **23**, 1334–1338 (2008).
9. B. Anasori, K.E. Sickafus, I.O. Usov, and M.W. Barsoum: Spherical nanoindentation study of the deformation micromechanisms of $LiTaO_3$ single crystals *J. Appl. Phys.* **110**, 023516 (2011).
10. A.G. Zhou, S. Basu, and M.W. Barsoum: Kinking nonlinear elasticity, damping and microyielding of hexagonal close-packed metals. *Acta Mater.* **56**, 60–67 (2008).
11. A.G. Zhou, D. Brown, S. Vogel, O. Yeheskel, and M.W. Barsoum: On the kinking nonlinear elastic deformation of cobalt. *Mater. Sci. Eng. A* **527**, 4664–4673 (2010).
12. M.W. Barsoum, A. Murugaiah, S.R. Kalidindi, T. Zhen, and Y. Gogotsi: Kink bands, nonlinear elasticity and nanoindentations in graphite. *Carbon* **42**, 1435–1445 (2004).
13. S. Basu and M.W. Barsoum: On spherical nanoindentations, kinking nonlinear elasticity of mica single crystals and their geological implications. *J. Struct. Geol.* **31**, 791–801 (2009).
14. A. Richter, B. Wolf, M. Nowicki, R. Smith, I.O. Usov, J.A. Valdez, and K. Sickafus: Multi-cycling nanoindentation in MgO single crystals before and after ion irradiation. *J. Phys. D, Appl. Phys.* **39**, 3342–3349 (2006).
15. W.C. Oliver and G.M. Pharr: Improved technique for determining hardness and elastic modulus using load and displacement sensing indentation experiments. *J. Mater. Res.* **7**, 1564–1583 (1992).
16. V.A. Coleman, J.E. Bradby, C. Jagadish, and M.R. Phillips: A comparison of the mechanical properties and the impact of contact induced damage in a- and c- Axis ZnO single crystals. *MRS Online Proc. Libr.* **957**, 0957-K07–17 (2006).
17. T. Saraswati, T. Sritharan, S. Mhaisalkar, C.D. Breach, and F. Wulff: Cyclic loading as an extended nanoindentation technique. *Mater. Sci. Eng. A* **423**, 14–18 (2006).

https://doi.org/10.1557/mrc.2013.39 Published online by Cambridge University Press